Pressure Compensation and the Bottom Boundary Layer

GEORGE L. MELLOR

Program in Atmospheric and Oceanic Sciences, Princeton University, Princeton, New Jersey

XIAO HUA WANG

Department of Geography and Oceanography, University College, Australia Defence Force Academy, Canberra, Australia

(Manuscript received 19 June 1995, in final form 15 March 1996)

ABSTRACT

It is an observed characteristic of oceans that velocities and horizontal pressure gradients are larger near the ocean surface than they are in deeper water. This is conventionally labeled "pressure compensation" whereby baroclinic structure, comprising sloping isopycnal surfaces, is adjusted so that surface pressure gradients are reduced in deeper water. In this paper, a two-dimensional flow in a channel is numerically modeled to demonstrate the baroclinic adjustment process and its relationship to the bottom boundary layer. A simple analytical model is also developed and defines the timescale of the adjustment process.

1. Introduction

It is observed that velocities are generally small in the deeper ocean. Thus, the geostrophically balanced velocity at the bottom is

$$f(u_H, v_H)$$

$$= \left(-g\frac{\partial\eta}{\partial x} - \int_{-H}^{0}\frac{\partial b}{\partial x}\,dz,\; g\frac{\partial\eta}{\partial y} + \int_{-H}^{0}\frac{\partial b}{\partial y}\,dz \right), \quad (1)$$

where u_H and v_H are zonal (x direction) and meridional (y direction) components of bottom velocity; η is the surface elevation; $b \equiv g\rho/\rho_0$ where ρ is density and ρ_0 is a reference density; f is the Coriolis parameter; g is the gravity constant; and $H(x, y)$ is the depth. In Eq. (1), small bottom velocities require that the surface pressure gradient be mostly balanced by the integral baroclinic terms. This balance is called pressure compensation.

In this paper we show that, in the simple case of channel flow, initially barotropic, the Ekman transport in the bottom boundary layer alters the overlying stratified flow such that pressure compensation is developed and the near-bottom velocities and stresses are reduced. Undoubtedly, the mechanism is at work in the real ocean. Whether or not it is a dominant mechanism is a question for further research.

The bottom boundary layer has received much less attention in the literature than the surface layer. There are nevertheless many papers; we cite a few examples. There are studies of the structure and turbulent nature of bottom layers (Armi and D'Asaro 1980) on flat and sloping bottoms (Weatherly and Martin 1978; Trowbridge and Lentz 1991); others deal with the lateral spreading of bottom layers (e.g., Jungclaus and Backhaus 1994). Some studies concern the impact of sloping bottom layers with emphasis on mixing and subsequent interior intrusion (e.g., Armi 1978; Phillips et al. 1986; Salmun et al. 1991), and there are papers that concern the role of bottom layers in coastal dynamics (e.g., Mellor 1986; Allen et al. 1995). The interaction of a cold filament on a sloping bottom was studied by Ezer and Weatherly (1990).

This paper was complete and reviewed when we tardily discovered the relevant papers by MacCready and Rhines (1991, 1993) and a review paper by Garrett et al. (1993). These papers treated local boundary layer processes on sloping topography; the timescale is on the order of a day or so. The present paper discusses the larger basin-scale flow development after the slope flow is "shut down;" the timescale is on the order of a year or more. The patient reader will see that a full discussion of the results of the aforementioned authors is best postponed to section 4 whence our results will have been presented.

2. Numerical experiments

To demonstrate the process of pressure compensation in the simplest context, consider a two-dimensional flow governed by

---

Corresponding author address: Prof. George L. Mellor, Program in Atmospheric and Oceanic Sciences, Princeton University, P.O. Box CN710, Sayre Hall, Princeton, NJ 08544-0710.
E-mail: glm@splash.princeton.edu

$$\frac{\partial u}{\partial x} + \frac{\partial w}{\partial z} = 0 \qquad (2)$$

$$\frac{\partial u}{\partial t} + \frac{\partial}{\partial x}(uu) + \frac{\partial}{\partial z}(wu) - fv$$

$$= -g\frac{\partial \eta}{\partial x} - \int_z^\eta \frac{\partial b}{\partial x}\,dz' + \frac{\partial \tau_{zx}}{\partial z} + F_u \qquad (3a)$$

$$\frac{\partial v}{\partial t} + \frac{\partial}{\partial x}(uv) + \frac{\partial}{\partial z}(uw) + fu = -g\frac{\partial \eta}{\partial y} + \frac{\partial \tau_{zy}}{\partial z} + F_v$$

$$(3b)$$

$$\frac{\partial \rho}{\partial t} + \frac{\partial}{\partial x}(u\rho) + \frac{\partial}{\partial z}(w\rho) = \frac{\partial q_z}{\partial z}, \qquad (3c)$$

which we will apply to a two-dimensional channel in the x–z plane. The positive x-direction is in the cross-shore direction; the positive y-direction is in the alongshore direction; z is positive upward. Apart from the symbols defined after Eq. (1), w is the vertical component of velocity, (τ_{zx}, τ_{zy}) are the Reynolds stresses, q_z is the density flux, and (F_u, F_v) are horizontal diffusion terms for momentum. In this paper, the horizontal diffusion term for density is null, a desirable attribute. However, some numerical noise will appear in the calculated results. The boundary conditions at the bottom are $w = u\partial H/\partial x$; the density flux is nil and the bottom stress is calculated by the model as detailed below. The surface boundary conditions are $w = u\partial \eta/\partial x + v\partial \eta/\partial y + \partial \eta/\partial t$. The system is driven by stipulating surface stress, density flux or the alongshore elevation gradient; in the experiments that follow the surface density flux is nil.

Equations (3a) and (3b) can be vertically integrated to obtain depth-averaged momentum equations and these are useful in interpreting the calculated results. The nonlinear momentum terms are at least an order of the magnitude less than other terms in the equations and can be neglected to simplify discussion but are not excluded in the following model experiments. After initial transients, the vertically integrated cross-shore velocity and tendency terms can also be neglected. Therefore,

$$-fD\bar{v} = -gD\frac{\partial \eta}{\partial x} - \int_{-H}^\eta \int_z^\eta \frac{\partial b'}{\partial x}\,dz'dz + \tau_{0x} - \tau_{Hx}$$

$$(4a)$$

$$0 = -gD\frac{\partial \eta}{\partial y} + \tau_{0y} - \tau_{Hy} + D\bar{F}_v \qquad (4b)$$

is the approximate balance of momentum terms for the numerical experiments that follow. In the above, $(\bar{u}, \bar{v})$ is the depth-averaged velocity, (τ_{0x}, τ_{0y}) is the surface wind stress, (τ_{Hx}, τ_{Hy}) is the bottom stress, and $D \equiv H + \eta \approx H$. In the numerical simulations, we stip-
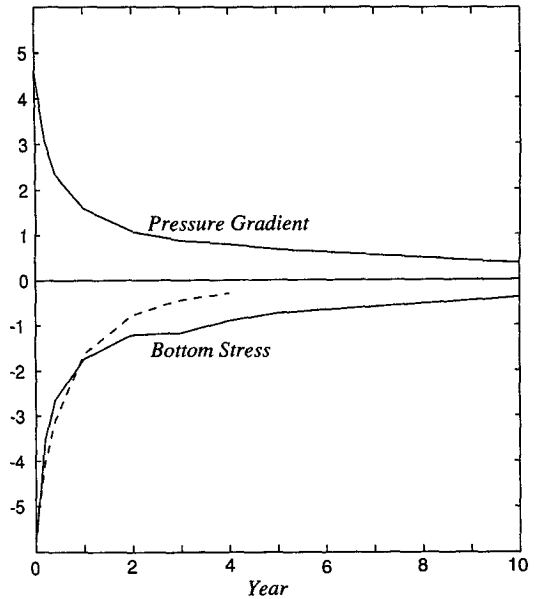

FIG. 1. Decay history for the alongshore pressure gradient, $-gH\partial\eta/\partial y$, and bottom stress, $-\tau_{Hy}$, at the center of the channel. Units are 10^{-4} m^2 s^{-2}. (Values computed at 20 years are about half those at 10 years.) The dashed curve is from Eq. (6c) for $\tau_b = 1.2$ yr.

ulate that the volume flow rate is stationary and, although $\partial D\bar{v}/\partial t$ is not zero locally, it is nevertheless small. We find that the horizontal friction term in (4b) is relatively small except in shallow water where it tends to reduce the bottom stress magnitude relative to the alongshore elevation gradient term.

The channel has an inverted bell shape (see Fig. 2), with a maximum depth of 4000 m and a surface width of 800 km. The time integration of the flow is obtained with a two-dimensional version of a numerical ocean model developed by Blumberg and Mellor (1980, 1987). The model uses a time-splitting algorithm for the external and internal modes. The external mode includes a free surface. In the x–z plane, the model uses a sigma-coordinate system so that Eqs. (2) and (3a–c) are first transformed to sigma coordinates before finite differencing. A turbulence closure scheme (Mellor and Yamada 1982) is used to simulate subgrid-scale mixing so that (τ_{zx}, τ_{zy}) and q_z can be obtained using model-calculated vertical eddy viscosities and diffusivities. The closure model produces logarithmic velocity profiles near the bottom that are matched to the law of the wall; the roughness parameter is taken to be 1 cm. The closure model has previously been used for bottom boundary layer studies by Weatherly and Martin (1978), Mellor (1986), Ezer and Weatherly (1991), Allen et al. (1995) and others. The horizontal eddy viscosity is calculated by the Smagorinsky diffusivity scheme with the constant $C = 0.2$. For details of the full, three-dimensional version of the ocean model, re-
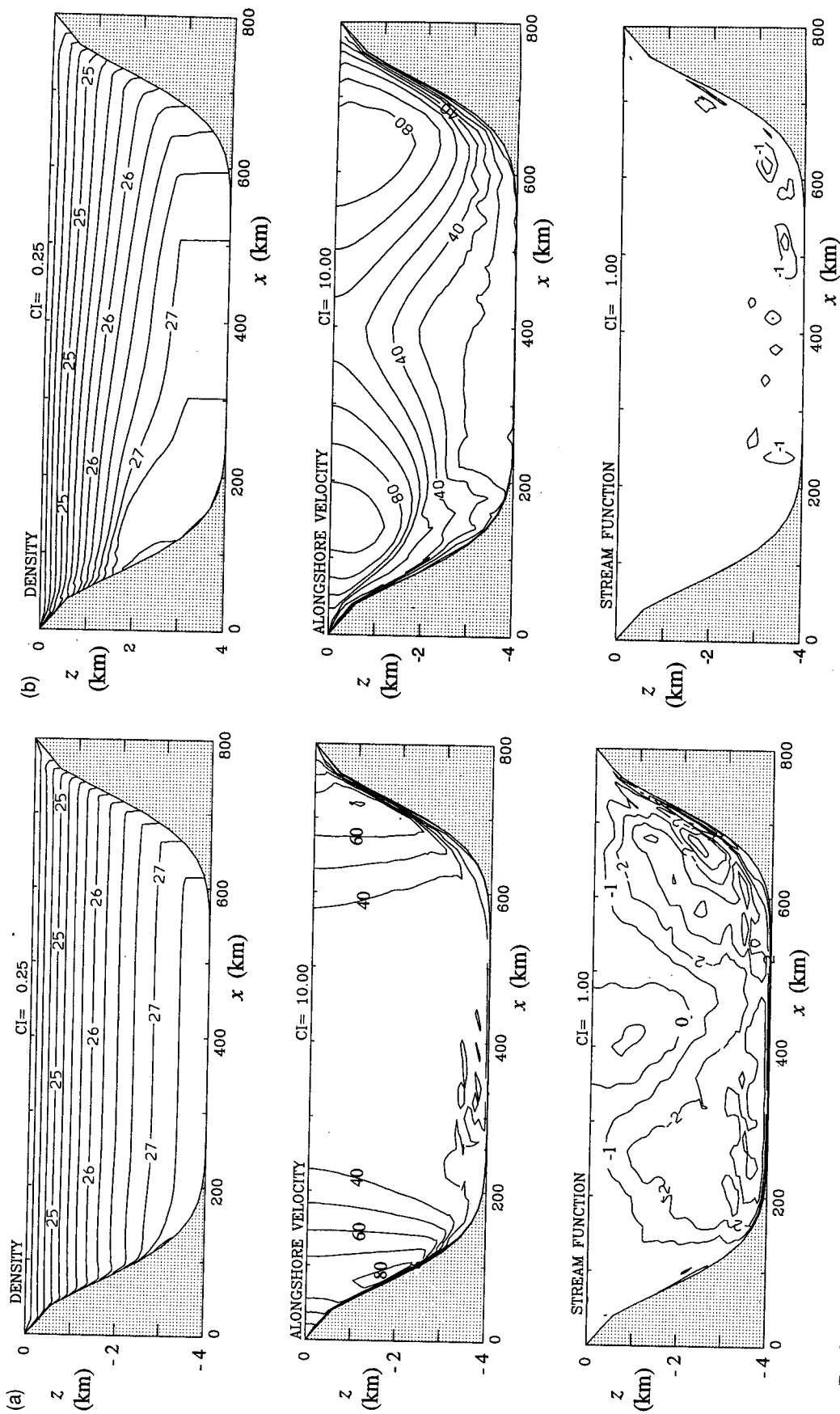
FIG. 2. (a) Density (sigma units), alongshore velocity (cm s^{-1}) and cross-shore stream function (m^2 s^{-1}) for the alongshore, elevation-gradient-driven flow at $t = 60$ days. The cross-shore elevation is nearly linear with respect to x and $\partial \eta / \partial x \approx 0.74 \times 10^{-5}$. (b) Same as Fig. 2a but for $t = 10$ years. Zero contours have been excluded. The cross-shore elevation is nearly linear with respect to x and $\partial \eta / \partial x \approx 0.56 \times 10^{-5}$.
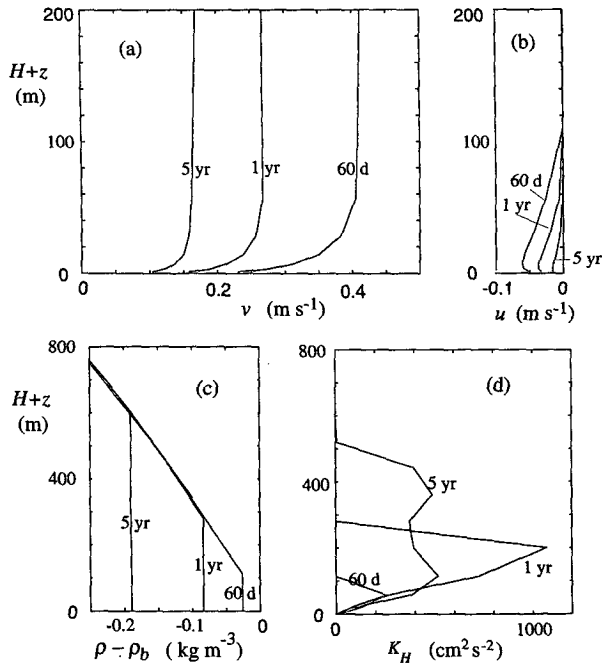
FIG. 3. Bottom boundary layer profiles at the center of the channel for the alongshore, elevation-gradient-driven flow at $t = 60$ days, 1 year, and 5 years. (a) Alongshore velocity. (b) Cross-shore velocities. (c) Density relative to the initial bottom density, ρ_b. (d) Mixing coefficient determined by the turbulence closure model.

fer to Blumberg and Mellor (1980, 1987) and Mellor (1992).

The present numerical simulations use a horizontal grid cell of 20 km in the x-direction and 60 sigma levels (calculated changes due to a reduction to 30 levels are quite small). Seven sigma levels are distributed logarithmically adjacent to the bottom and surface. The initial density distribution is

$$\rho = \left[1028 - 4 \exp\left(\frac{z}{2000 \text{ m}}\right) \right] \text{kg m}^{-3} \quad (5)$$

and $f = 10^{-4}$ s^{-1}. The first baroclinic Rossby radius of deformation is 36 km.

a. Flow driven by an alongshore elevation gradient

In this simulation, the surface wind stress (τ_{0x}, τ_{0y}) is equal to zero. An initial alongshore velocity of v = 50 cm s^{-1} is specified. Thereafter, the alongshore elevation gradient, $\partial\eta/\partial y = F(t)$, is adjusted by the computer code to maintain a constant volume flow rate. To reduce the integration time, the alongshore velocity is quite large; however, the western part of the flow will have some resemblance to the Gulf Stream along the South Atlantic Bight.

Figure 1 shows the 10-year variation of the along-shore pressure gradient and bottom stress at the center

of the channel. As indicated by (4b) for small horizontal friction, the pressure gradient is balanced by the bottom stress. The bottom velocities and stresses decrease in time; the alongshore elevation is decreased to maintain a constant flow rate.

Figures 2a and 2b show the surface elevation, the density, the alongshore velocity, and the streamfunction ($u = \partial\psi/\partial z$, $w = -\partial\psi/\partial x$) for day 60 and year 10, respectively. On day 60, near the beginning of the integration, the density is little changed from the initial state, and a cross-shore slope of surface elevation has developed so that the alongshore velocity is nearly geostrophically balanced. The alongshore velocity is almost vertically uniform although flows on the shelves and immediately near the bottom are reduced due to bottom friction. The bottom friction has created a bottom boundary layer, which drives a westward Ekman transport. This westward bottom flow upwells into the western interior, then downwells in the east and is reentrained in the bottom boundary layer forming the vertical circulation cell shown in the lower panel of Fig. 2a.

Details of the boundary layer at the center channel bottom are displayed in Fig. 3. Cross-shore velocities reach a maximum of 6.5 cm s^{-1} at about 10 m above the seabed (Fig. 3b). The resultant tilting of the overlying isopycnals reduces the alongshore velocity (Fig. 3a). On the downwelling side of the basin, the bottom boundary is statically unstable (Weatherly and Martin 1978; Trowbridge and Lentz 1991). Thus, in the early stages, the mixing coefficient at a depth of 3000 m on the eastern side is about double, in magnitude and penetration, than that for the western side (not shown). In the middle of the channel, the importation of lower density water from the east (Fig. 3c) results in increased mixing (Fig. 3d). In the latter stages, mixing is very small on the western slope but large on the eastern slope and on the flat bottom. This explains why the boundary thickness for density is greater than that for velocity as seen in Fig. 2b and Fig. 3. The velocity boundary layer is essentially a neutral layer and its thickness is limited by a Coriolis, stress divergence balance and conforms to the well known rule, $\delta \approx 0.4 f^{-1}\sqrt{\tau_H/\rho_0}$; using the calculated bottom stress at $t = 60$ d, one obtains $\delta \approx 100$ m.

After 10 years, Fig. 2b shows how the density structure has changed. Isopycnals have tilted in a direction opposite to the surface elevation slope and the deepest velocities are reduced, in accordance with Eq. (1), from about 40 cm s^{-1} on day 60 to about 10 cm s^{-1} after 10 years. The surface velocities increase from 50 cm s^{-1} to about 75 cm s^{-2} after 10 years so that a constant volume flow rate along the channel is maintained. A pair of current jets have also been formed above western and eastern slopes. Due to reduced bottom velocity and therefore diminished bottom stress, the cross-shore circulation is diminished as indicated by the boundary layer profiles in Fig. 3 and the lower
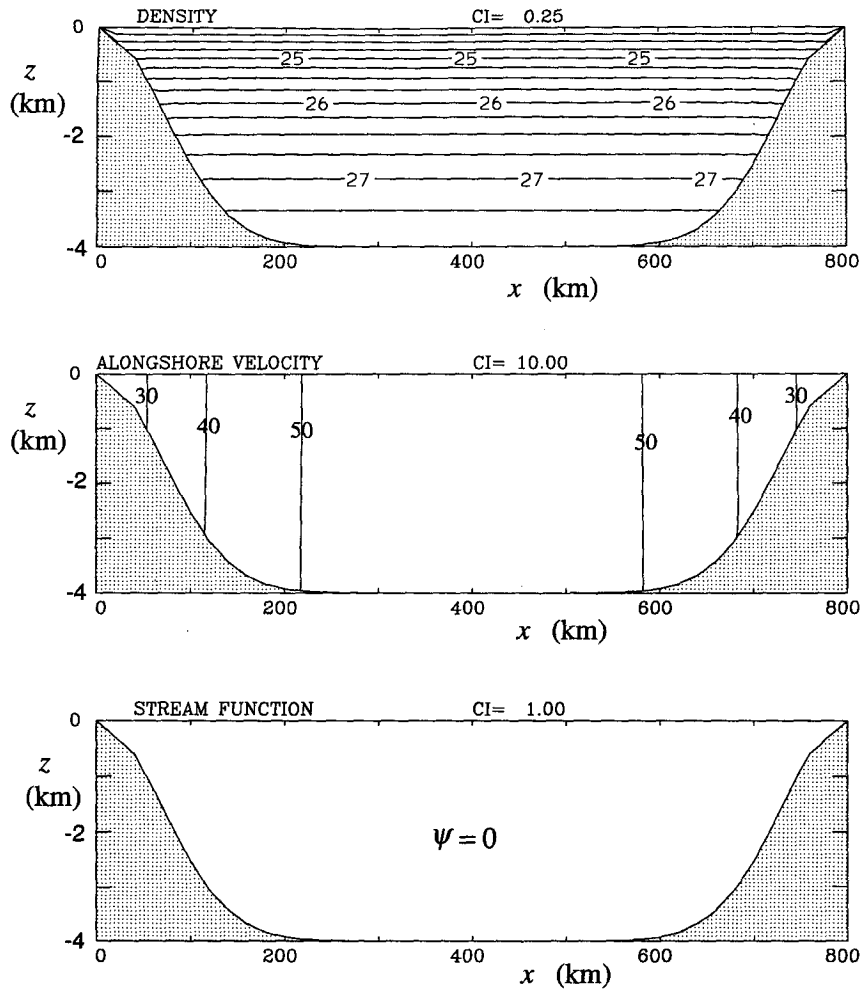
FIG. 4. Control run at $t = 10$ yr. Same as Fig. 2b but with free slip at the bottom.

panel of Fig. 2b. The calculation was continued for an additional ten years with a bottom free-slip condition (not shown); the bottom velocity increases from about 20 cm s^{-1} to 40 cm s^{-1} and the jetlike structure in Fig. 2b vanishes. In the absence of horizontal diffusion, the density structure changes are barely discernible.

To make it clear that a bottom boundary layer is responsible for the adjustment of the baroclinic field, a control run with a free slip, bottom boundary condition was executed. Figure 4 shows density and alongshore velocity after 10 years (and is nearly identical to the 20 year result) with the same initial conditions used in the experiment discussed above. Since there is no bottom friction, there is no cross-shore Ekman transport near the bottom and no tilting of the isopycnals, therefore the density structure remains unchanged and a barotropic velocity is sustained.

b. Flow driven by an alongshore surface stress

Other than surface density flux, the only way to drive our two-dimensional system is either to impose an alongshore elevation gradient, as we have demonstrated above, or to impose a surface stress. The latter differs from the former in that it creates a cross-shore, surface Ekman transport. This could compete with the bottom Ekman transport in altering the interior baroclinic structure. Therefore, we have run another numerical experiment wherein the alongshore elevation gradient is nil and we impose an alongshore stress, $(\tau_{0y}, \tau_{0x}) = (\tau_0(t), 0)$. Once again, to maintain a time-independent volume flow rate in the channel, the surface stress is adjusted to maintain a constant flow rate. Since the alongshore pressure gradient has been turned off, the wind stress is balanced by the bottom stress τ_{Hy}, as dictated by Eq. (4b) for small horizontal friction. The other conditions remain unchanged. Figure 5
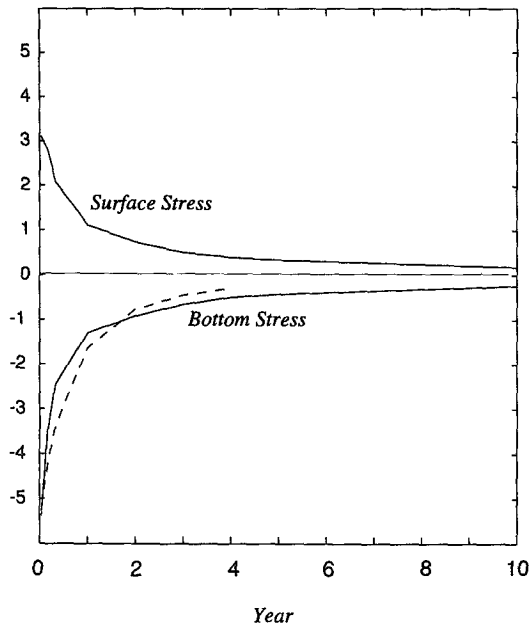
FIG. 5. Decay history for the alongshore wind stress τ_{0y} and bottom stress τ_{Hy} at the center of the channel. Units are 10^{-4} m^2 s^{-2}.

shows the 10-year variation of the alongshore surface and bottom stresses at the center of the channel. Again, both stresses decrease with time and asymptote to zero. Figures 6a and 6b show the density, alongshore flow and a streamfunction plot after 60 days and 10 years of integration. Now the bottom Ekman transport, about 3 m^2 s^{-1}, continues to the surface where it is entrained in the surface Ekman layer. For the deep and intermediate depths the tilting of the isopycnals is about the same as in the elevation-gradient-driven flow. After 10 years, the bottom velocity is largely reduced due to the pressure compensation, as seen in Fig. 6b. This reduction of bottom velocity causes a diminished bottom stress and the externally adjusted surface stress also decreases to maintain constant flow.

We have again executed a control run with free slip at the bottom so that there is no bottom boundary layer; the results are not significantly different from that of Fig. 4 and are not shown.

3. A simple analytical model

A simple two-dimensional model for a two-layer, rectangular channel is depicted in Fig. 7. Two regions of constant but differing densities are separated by an isopycnal interface. As in the model of section 2a, the flow is initially barotropic and $v_1 = v_2 = v_{20}$. Thereafter, as suggested by Fig. 2b, the interface is modeled as a straight line and the ageostrophic bottom boundary layer causes a tilting of the interface and a reduction in v_2 relative to v_1 during which

time the total flow rate, $v_1 H_1 + v_2 H_2$, is maintained constant. The detailed analysis is contained in the appendix and the results are

$$v_2 = \frac{v_{20}}{1 + A|v_{20}|t}, \qquad A \equiv \frac{2C_d g' H_1}{f^2 L^2 H}, \qquad (6a,b)$$

and the bottom stress is

$$\frac{\tau_{Hy}}{\tau_{Hy0}} = \left(\frac{1}{1 + A|v_{20}|t}\right)^2 = \left(\frac{1}{1 + t/\tau_b}\right)^2. \qquad (6c)$$

The basin timescale is therefore

$$\tau_b = \frac{1}{A|v_{20}|} = \frac{H}{2C_d|v_{20}|}\frac{L^2}{R^2}, \qquad (7)$$

where $R = \sqrt{g'H_1}/f$ is the internal Rossby radius of deformation. For the experiment discussed in section 2a, we have $v_{20} = 0.5$ m s^{-1}, $C_d = 0.0022$, $H = 4000$ m, $R = 36$ km, and $L \approx 400$ km so that $\tau_b = 0.72$ yr. The bottom drag coefficient, C_d, is referenced to the geostrophic velocity above the bottom boundary layer and was obtained diagnostically from the numerical experiment in section 2. The dashed curve in Fig. 1 is from Eq. (6c) for $\tau_b = 1.2$ yr but the choice of the "best" value is subjective; nevertheless, a good fit to the bottom stress in Fig. 1 is obtained for the first few years after which the numerical solution decays more slowly; this may be due to the small amount of lateral friction in the numerical solution or to other simplifications in the analytical model. However, these details aside, one must conclude that (7) is a good estimate of the basin timescale of the baroclinic adjustment process.

4. The early stage

Thus far, this paper has been concerned with long timescale processes. We now examine details of a much shorter timescale process.

The idea that bottom boundary Ekman transport can interact with the overlying water so that the near-bottom velocity is reduced is contained in papers by MacCready and Rhines (1993) and Garrett et al. (1993). This has been dubbed a "slippery water" phenomenon since the reduced bottom velocity results in reduced bottom stress. (The term, slippery water, has also been used to describe a physically distinct process wherein polymers have been added to water to reduce turbulence and drag coefficients; in the present usage the drag coefficient, for example, is not effected.) These papers treat the development of boundary layers on sloping topography. To make the connection with the present calculations, we examine details of the flow in the early spinup stages. Thus, in Fig. 8, flow properties are plotted for the slope at $x = 110$ km where $H = 3050$ and $dH/dx = 0.023$. The ordinate is the depth measured from the bottom and profiles are provided from 1 to 5 days. To eliminate inertial oscillations, the flow has been ramped up linearly from rest over an inertial
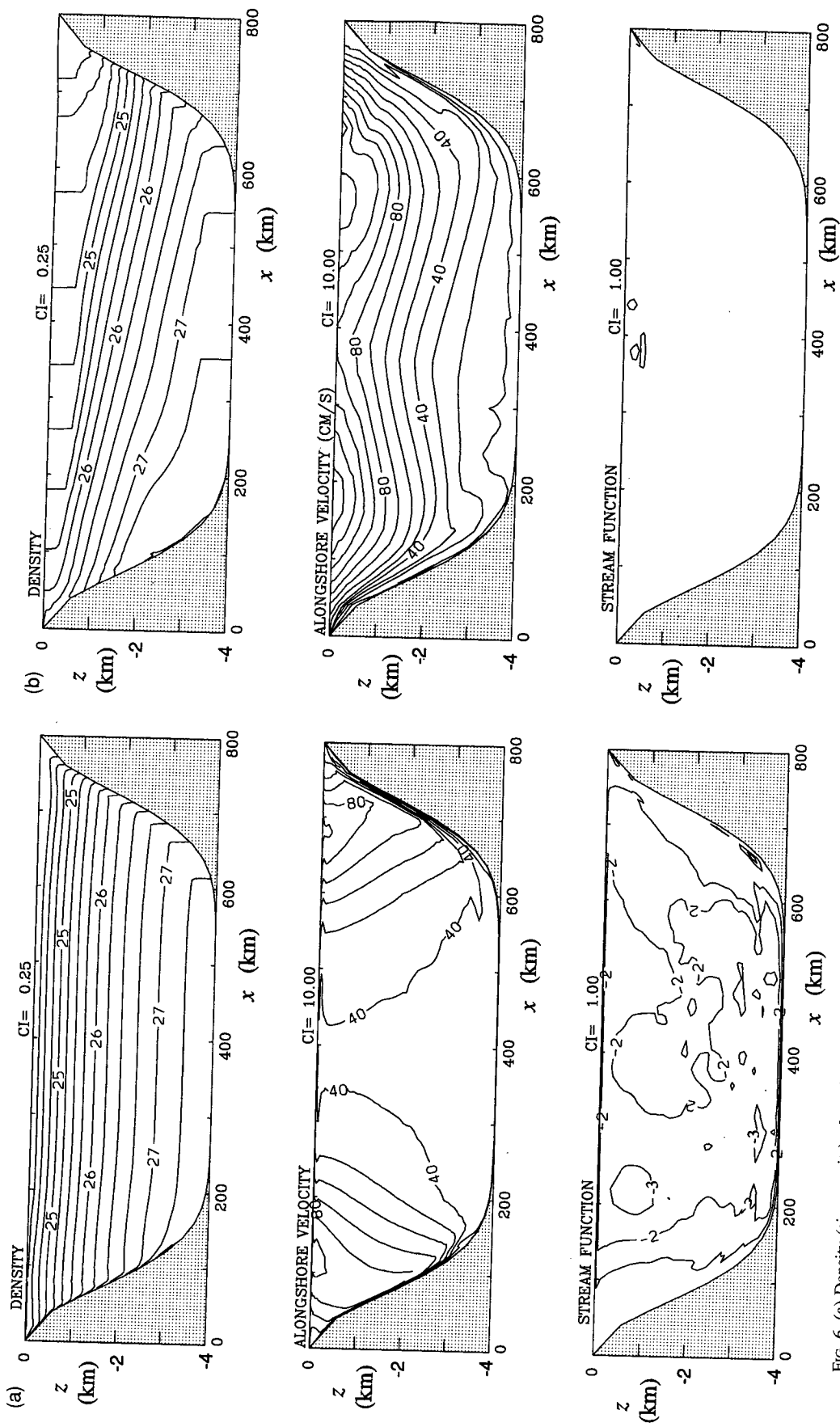
FIG. 6. (a) Density (sigma units), alongshore velocity (cm s⁻¹) and cross-shore stream function (10^6 m² s⁻¹) for the wind-driven flow at $t = 60$ days. (b) Same as Fig. 6a at $t = 1$ yr.

period of 18 hours after which the volume flow through the channel is held constant.

In Fig. 8, it will be observed that the cross-slope flow (Fig. 8b) accelerates from rest and transports denser water upslope (Fig. 8c). The adverse pressure gradient caused by the heavy water anomaly then "shuts down" the upslope flow and the process is arrested. Meanwhile, the overlying water has been altered to effect local pressure compensation and reduce the alongslope velocity near the bottom (Fig. 8a). The timescale for the flow to be arrested according to MacCready and Rhines (1993) is

$$\tau_s = \frac{f}{(\alpha N)^2}, \tag{8}$$

which represents a balance between Coriolis acceleration and the buoyancy force anomaly due to the upslope transport of density; here $\alpha \equiv dH/dx$. For the parameters of the problem of this paper, $\tau_s = 20$ h. The shutdown time seen in Fig. 8 is several days. Note that the bottom boundary layers on the shallow portions of the slope are arrested first (not shown) and are then followed by the deeper portions.

We now can see that the arrested slope boundary layer process is a precursor to the larger scale processes that occur for $t \gg \tau_s$. After these boundary layers are arrested, Fig. 2a shows that, on the upwelling side, the flow separates just after the point where the flat bottom melds into the sloping bottom. Thereafter, the slope water is not a primary participant in the basin-scale flow development (note that the simple model advanced in section 3 has vertical side walls). The governing timescale is the basin scale given by Eq. (7) which, for the present problem is of the order of a year.

FIG. 8. An examination of the spinup details on the slope at x = 110 km where $H = 3052$ m. (a) Alongshore velocity. (b) Cross-shore velocity. (c) Density after subtraction of the initial density. (d) The vertical mixing coefficient developed by the turbulence closure submodel. The labels on the curves denote days.

4. Conclusions

Bottom boundary layers are formed if finite bottom velocities exist. Bottom Ekman transport tilts the isopycnals and cancels the surface pressure gradient. This process results in a vanishing deep ocean flow and bottom boundary layer stress. Although we have only demonstrated the process for a channel flow, a proposition is that, in real oceans, the bottom boundary layer may be responsible or, at least, contribute to the creation and maintenance—with yearly timescales—of greatly reduced deep water velocities and small horizontal pressure gradients relative to those at the surface. An interpretation of Fig. 2a, (Csanady and Pelegri 1995) is that potential vorticity, $f\partial\rho/\partial z$, is advected from the bottom boundary layer into the interior on the upwelling side of the channel and then advected from the interior to the bottom boundary on the downwelling side.

If one is concerned with perturbations around an existing equilibrium state with initially small geostrophic velocity near the bottom, then the effective v_{20} is relatively small and τ_b relatively large according to Eq. (7). More research is obviously needed to further evaluate the process.
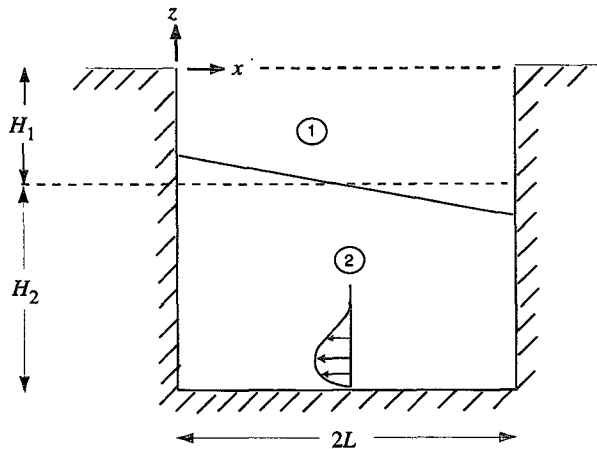
FIG. 7. A simple model illustrating the tilting of an isopycnal due to ageostrophic flow in the bottom boundary layer of a two layer model. Region 1 and 2 are regions of constant density. The density difference is $\delta\rho = \rho_2 - \rho_1$.
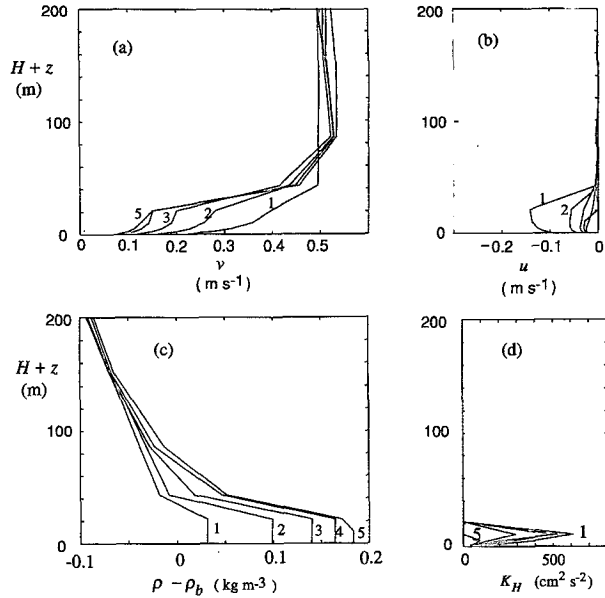
APPENDIX

Derivation of Equation (6)

With reference to Fig. 7, let $h(x)$ be the displacement of the isopycnal interface assumed to be a straight line. Simple geometric considerations yield a conservation of mass expression

$$\frac{L^2}{2} \frac{\partial}{\partial t} \left(\frac{\partial h}{\partial x} \right) = Q_b = \frac{\tau_{Hy}}{f}, \tag{A1}$$

where Q_b is the bottom Ekman transport. The second identity is the well-known relation between the transport and bottom stress. The stress is related to velocity according to $\tau_{Hy} = C_d |v_2| v_2$ so that

$$\frac{\partial^2 h}{\partial t \partial x} = \frac{2 C_d}{f L^2} v_2 |v_2|. \tag{A2}$$

The top and bottom alongshore flow is geostrophically balanced by the cross-shore pressure gradient so that

$$-f v_1 = -g \frac{\partial \eta}{\partial x}, \quad -f v_2 = -g \frac{\partial \eta}{\partial x} - g' \frac{\partial h}{\partial x}. \tag{A3a,b}$$

Subtraction of (A3a) from (A3b) yields the Witte–Margulies relation

$$f(v_1 - v_2) = g' \frac{\partial h}{\partial x}. \tag{A4}$$

The alongshore flow rate is constant with time so that

$$H_1 \frac{\partial v_1}{\partial t} + H_2 \frac{\partial v_2}{\partial t} = 0. \tag{A5}$$

Combining (A2), (A4), and (A5) then yields

$$\frac{\partial v_2}{\partial t} + A v_2 |v_2| = 0, \tag{A6}$$

where $A \equiv 2 C_d g' H_1 / (f^2 L^2 H)$. Equations (6a,b) follows from (A6).

REFERENCES

Allen, J. S., P. A. Newberger, and J. Federiuk, 1995: Upwelling circulation on the Oregon continental shelf. Part I: Response to idealized forcing. *J. Phys. Oceanogr.,* **25,** 1843–1866.

Armi, L., 1978: Some evidence for boundary mixing in the deep ocean. *J. Geophys. Res.,* **83,** 1971–1979.

——, and E. D'Asaro, 1980: Flow structures of the benthic ocean. *J. Geophys. Res.,* **85,** 469–484.

Blumberg, A. F., and G. L. Mellor, 1980: A coastal ocean numerical model. *Proc. Int. Symp. Mathematical Modelling of Estuarine Physics,* J. Sunderman and K.-P. Holts, Eds., Springer-Verlag, 203–214.

——, and ——, 1987: A description of a three-dimensional coastal ocean circulation model. *Three-Dimensional Coastal Ocean Models,* Vol. 4, H. Heaps, Ed., Amer. Geophys. Union, 1–16.

Csanady, G. T., and J. L. Pelegri, 1995: Vorticity balance of boundary currents. *J. Mar. Res.,* **53,** 171–187.

Ezer, T., and G. L. Weatherley, 1990: A numerical study of the interaction between a deep cold jet and the bottom boundary layer of the ocean. *J. Phys. Oceanogr.,* **20,** 801–816.

Garrett, C., P. MacCready, and P. Rhines, 1993: Boundary mixing and arrested Ekman layers: Rotating stratified flow near a sloping boundary. *Annual Reviews of Fluid Mechanics,* Vol. 25, Annual Reviews, 291–325.

Jungclaus, J. H., and J. O. Backhaus, 1994: Application of a transient reduced gravity plume model to the Denmark Strait Overflow. *J. Geophys. Res.,* **99,** 12 375–12 396.

MacCready, P., and P. Rhines, 1991: Buoyant inhibition of Ekman transport on a slope and its effect on stratified spin-up. *J. Fluid Mech.,* **223,** 631–661.

——, and ——, 1993: Slippery bottom boundary layers on a slope. *J. Phys. Oceanogr.,* **23,** 5–22.

Mellor, G. L., 1986: Numerical simulation and analysis of the mean coastal circulation off California. *Contin. Shelf Res.,* **6,** 689–713.

——, 1992: User's guide for a three-dimensional, primitive equation numerical ocean model. Report: Program in Atmos. and Ocean. Sci., Princeton University, Princeton, NJ 08544, 35 pp.

——, and T. Yamada, 1982: Development of a turbulence closure model for geophysical fluid problems. *Rev. Geophys. Space Phys.,* **20,** 851–875.

Phillips, O. M., J.-H. Shyu, and H. Salmun, 1986: An experiment on boundary mixing: Mean circulation and transport rates. *J. Fluid Mech.,* **173,** 473–499.

Salmun, H., P. D. Killworth, and J. R. Blundell, 1991: A two-dimensional model of boundary mixing. *J. Geophys. Res.,* **96,** 18 447–18 474.

Trowbridge, J. H., and S. J. Lentz, 1991: Asymetric behavior of the oceanic boundary layer above a sloping bottom. *J. Phys. Oceanogr.,* **21,** 1171–1185.

Weatherly, G. L., and P. J. Martin, 1978: On the structure and dynamics of the ocean bottom boundary layer. *J. Phys. Oceanogr.,* **8,** 557–570.